

Pulsations and Period Changes in the double-mode SX Phoenicis Star AE Ursae Majoris

J. S. Niu

Astronomy Department, Beijing Normal University, Beijing 100875, China

J. N. Fu¹

Astronomy Department, Beijing Normal University, Beijing 100875, China

X. H. Yang

Astronomy Department, Beijing Normal University, Beijing 100875, China

W. K. Zong

Astronomy Department, Beijing Normal University, Beijing 100875, China

Received _____; accepted _____

ABSTRACT

Time-series photometric observations were made for the SX Phoenicis star AE UMa between 2009 and 2012 at the Xinglong Station of National Astronomical Observatories of China. With the frequency analysis of the light curves, we confirmed the fundamental and the first overtone frequencies as $f_0 = 11.62560 \text{ c d}^{-1}$ and $f_1 = 15.03124 \text{ c d}^{-1}$. Additionally, we got 37 frequencies which are identified as the harmonics and the combinations of the fundamental and first overtone frequencies. 25 of which are newly detected. No frequencies of the other pulsation modes were found. The $O - C$ diagram, produced from 84 newly determined times of maximum light combined with those derived from the literature, reveals a continuous period variation with the rate of $(1/P_0)(dP_0/dt) = 5.4(8) \times 10^{-9} \text{ yr}^{-1}$ and $(1/P_1)(dP_1/dt) = -2.8(4) \times 10^{-8} \text{ yr}^{-1}$. Theoretical rates of period change due to the stellar evolution were calculated with the modeling code MESA. The result shows that the observed rate of period change is fully consistent with period change caused by the evolutionary behavior predicted by standard theoretical model. Constraint of the variation of P_1 allows us to determine the star's location on the H-R diagram precisely with the mass $1.72(\pm 0.06) M_\odot$ and the age $1.4(\pm 0.2) \times 10^9 \text{ yr}$.

Subject headings: stars: variables: SX Phe — stars: individual: AE UMa — stars: evolution: MESA — techniques: photometric

1. INTRODUCTION

δ Scuti stars are a class of pulsating variable stars that lies in the classical instability strip crosses the main sequence on the Hertzsprung-Russell diagram, whose pulsations are driven by the κ -mechanism which drives both the Cepheids and the RR Lyrae stars as well. With masses between 1.5 and 2.5 M_{\odot} , periods between 0.03 and 0.3 *days*, luminosities between 10 and 50 L_{\odot} , these stars pulsate with amplitudes from mmag up to tenths of a magnitude.

The high-amplitude δ Scuti stars (hereafter HADS) are traditionally found to be slow rotators with one or two dominant radial modes with amplitudes larger than 0.1 mag, although they may occasionally have low-amplitude, non-radial modes in addition to the main pulsation modes (Poretti (2003)). It is interesting to probe whether it is an overall property of all HADS.

SX Phoenicis (SX Phe) stars, a subgroup of HADS, are old Pop. II stars. Because of the insufficient amount and the poor photometric precision of the observation data, whether any low-amplitude pulsations exist besides the dominant radial modes in most SX Phe stars are unknown. According to the existing data, they could probably be either in a post-giant branch stage of evolution or merged binary stars (Rodríguez & López-González (2000)). Although most SX Phe stars, which are characterized by high amplitudes of pulsation, low metallicity, and large spatial motion, are found to be members of globular clusters (Rodríguez & López-González (2000)), some of them have been discovered in the general star fields (Rodríguez & Breger (2001)). Particularly, pulsations in the majority of the field SX Phe variables display very simple frequency spectra with short periods ($\leq 0^{\text{d}}.08$) and large visual peak-to-peak amplitudes ($\geq 0^{\text{m}}.1$, c.f. Fu et al. (2008)). Precise time-series photometric observations reveal period changes in these stars, which should

¹Send offprint request to: jnfu@bnu.edu.cn

theoretically reflect the evolutionary changes in radius. Rodríguez et al. (1995) collected observed period changes found in some HADS (including SX Phe stars) and indicated that sudden jumps of period could be an explanation for the period changes observed in the SX Phe stars. Additionally, the study of period changes of double-mode SX Phe stars raises a further important question: how does the overtone frequency change? From a simple theoretical consideration, one could guess that the fundamental and overtone frequencies of radially pulsating SX Phe stars change in the same direction and at about the same rate. However, the star we study in this paper, AE UMa, has the fundamental and first overtone frequencies changed neither in the same direction nor at the same rate (Pócs & Szeidl (2001), Zhou (2001)). Therefore, it is interesting to investigate pulsation behaviors of this star with the extended data of improved photometric precision.

The star AE Ursae Majoris (hereafter AE UMa)(= HIP 47181, $\alpha_{2000} = 09^h36^m53^s$, $\delta_{2000} = 44^\circ04'01''$, $\langle V \rangle = 11^m.27$, $P_0 = 0^d.0860$, $\Delta V = 0^m.10$, A9), was discovered by Geyer et al. (1955). The spectral type of AE UMa was classified by Götz & Wenzel (1961) as A9 in accordance with the type of variability. Until 1973, it was shown that the star had significant light-curve variation with the determination of the period of the light variation and the type of variability as dwarf Cepheid (Tsesevich (1973)). Then, the 1974 Konkoly observations found the beat phenomenon (Szeidl (1974)). In 1995, the star is listed as an SX Phe star in Garcia et al. (1995). However, Hintz et al. (1997a) showed strong evidence against this classification, and reclassified it as a normal Population I, high-amplitude δ Scuti star. According to the calculation of Breger & Pamyatnykh (1998), AE UMa had such fast period decreasing ($48 \times 10^{-8} \text{ yr}^{-1}$) only if it was a pre-MS star, but there exists no evidence that it is a pre-MS star. At last, both Pócs & Szeidl (2001) and Zhou (2001) analyzed pulsations of the star with better and longer data sets, and the results rejected the outcomes from Hintz et al. (1997a). AE UMa was classified as a Pop. II, post-MS SX Phe

star once again, with the fundamental frequency stable and the first overtone decreasing with a rate of about 10^{-8} yr^{-1} .

In the following sections, we present a detailed study of the period changes of AE UMa, mainly based on extended time-series CCD observations from 2009 to 2012 collected at the Xinglong Station of National Astronomical Observatories of China (NAOC). The organization of the paper is: Section 2 describes observations and data reduction; Section 3 introduces the pulsation analysis of the new data; Section 4 discusses the variations of the periods; Section 5 calculates the models with the constraints of the frequencies and their variations; Section 6 lists our conclusions.

2. OBSERVATIONS AND DATA REDUCTION

Photometric observations for AE UMa were made with the 85-cm telescope located at the Xinglong Station of NAOC between March 2009 and May 2012. The 85-cm telescope is equipped with a standard Johnson-Cousin-Bessel multicolour filter system and a PI1024 BFT CCD camera mounted on the primary focus ((Zhou et al. 2009)). The CCD camera has 1024×1024 pixels, corresponding to a field of view of $16.5' \times 16.5'$. Since March 2012, the CCD camera has been replaced by a PI512 BFT, which has 512×512 pixels corresponding to a field of view of $15' \times 15'$. The observations were made through a standard Johnson V filter with the exposure time ranging from 15 to 120 seconds, depending on the atmospheric conditions. A journal of the new observations is listed in Table 1.

In total, more than 17277 CCD frames of data were collected for AE UMa within 40 nights. Figure 1 shows an image of AE UMa taken with the 85-cm telescope, where the comparison star (TYC 2998-1249-1) and the check star (TYC 2998-1166-1) are marked.

CCD	Year	Month	Nights	Frames
PI BFT1024	2009	Mar	5	4055
	2009	May	3	516
	2010	Feb	2	1385
	2011	Jan	5	1275
	2011	Feb	8	4759
	2012	Jan	1	328
	2012	Feb	6	1887
PI BFT512	2012	Mar	5	2516
	2012	Apr	5	556

Table 1: Journal of observations with the 85-cm telescope.

The coordinates and the brightness in V of the two stars are listed in Table 2. After bias, dark and flat-field corrections, aperture photometry was performed by using the DAOPHOT program of IRAF. The light curves were then produced by computing the magnitude differences between AE UMa and the comparison star. The standard deviations of the magnitude differences between the check star and the comparison star yielded an estimation of photometry precisions, with the typical value of $0^m.003$ in good observation conditions and $0^m.011$ in poor cases. Although there were slight zero-point shifts, we adjusted it with the fit light curves of the data for every month (assuming the frequencies are stable in a month).

Table 2: The comparison star and the check star used in the photometry of AE UMa

Star name	$\alpha(2000)$	$\delta(2000)$	V
Comparison = TYC 2998-1249-1	$09^h37^m28^s.5826$	$+44^\circ01'16''.854$	11.334
Check = TYC 2998-1166-1	$09^h37^m12^s.058$	$+43^\circ58'20''.12$	12.215

Table 2: Comparison and check stars

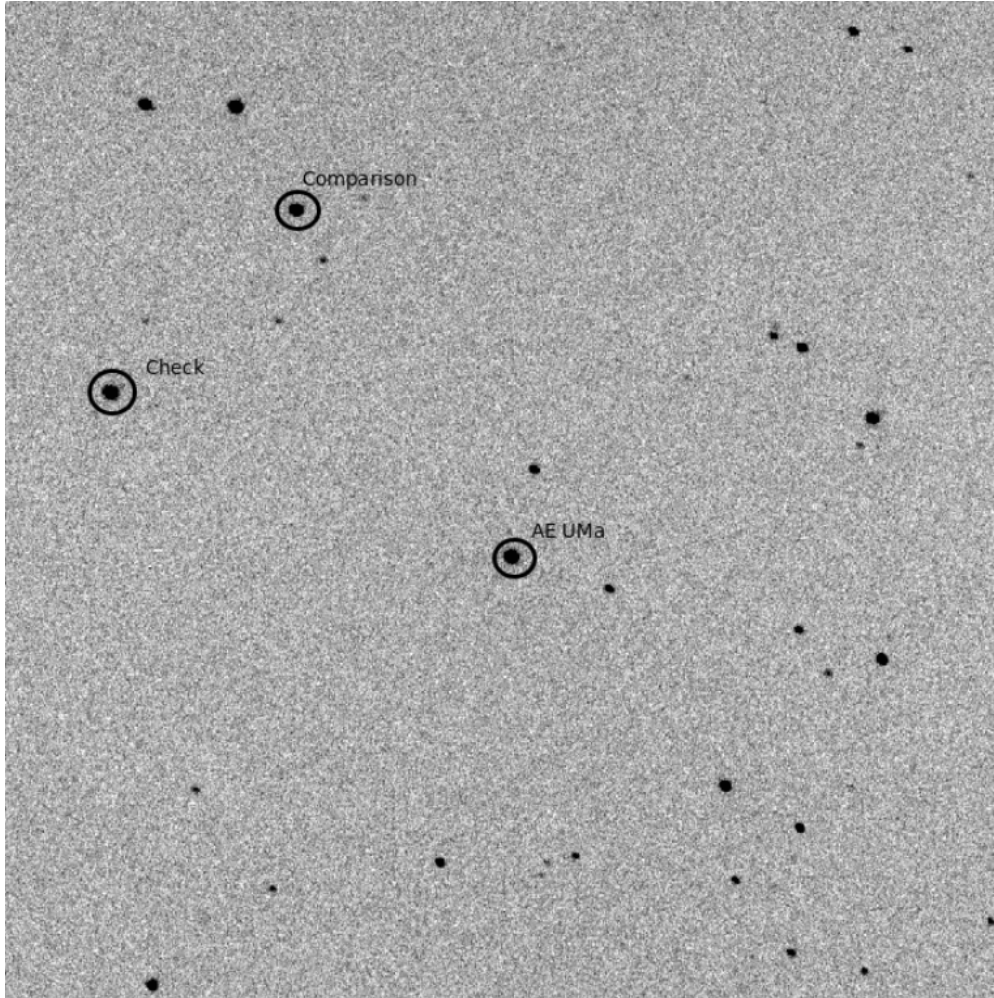


Fig. 1.— A CCD image ($16.5' \times 16.5'$) of AE UMa ($\alpha_{2000} = 09^{\text{h}}36^{\text{m}}53^{\text{s}}$, $\delta_{2000} = +44^{\circ}04'00''$) taken with the 85-cm telescope at the Xinglong Station. North is down and East is to the right. AE UMa, the comparison and the check star are marked.

Figure 2 shows the light curves of AE UMa in Johnson V band observed with the 85-cm telescope in 2009, 2010, 2011 and 2012, which was used to make frequency analysis.

3. PULSATION ANALYSIS

Frequency analysis was performed with the light curves of AE UMa in the years 2009, 2010, 2011 and 2012, respectively with the software PERIOD04 (Lenz & Breger (2005)), which makes Fourier transformations of the light curves to search for significant peaks in the amplitude spectra. Then, the light curves are fitted with the following formula

$$m = m_0 + \Sigma A_i \sin(2\pi(f_i t + \phi_i)). \quad (1)$$

In Table 3 was listed the solutions of up to 37 frequencies whose signal-to-noise ratios (S/N) are larger than 4.0 (Breger et al. (1993)). The solid curves in Figure 2 show the fits with the frequency solutions in different years. From Table 3, one notes that the 37 frequencies are composed of the fundamental and the first overtone frequencies, their harmonics and linear combinations. As can be noticed, no significant signals are detected in addition to these frequencies.

Figure 3 and Figure 4 show the window functions from 2009 to 2012 and the amplitude spectra of the frequency pre-whitening process for the light curves in V observed in 2009 with the 85-cm telescope at Xinglong station of NAOC respectively.

As can be seen from Figure 2, the constructed curves fit well the observed light curves collected in 2009, 2010, 2011 and 2012, which shows that the fundamental and the first overtone frequencies, their harmonics and linear combinations can explain the pulsation behavior of AE UMa.

To show the variations of frequencies and amplitudes of pulsations of the star, we compare our results with those from Zhou (2001). who collected data for AE UMa from

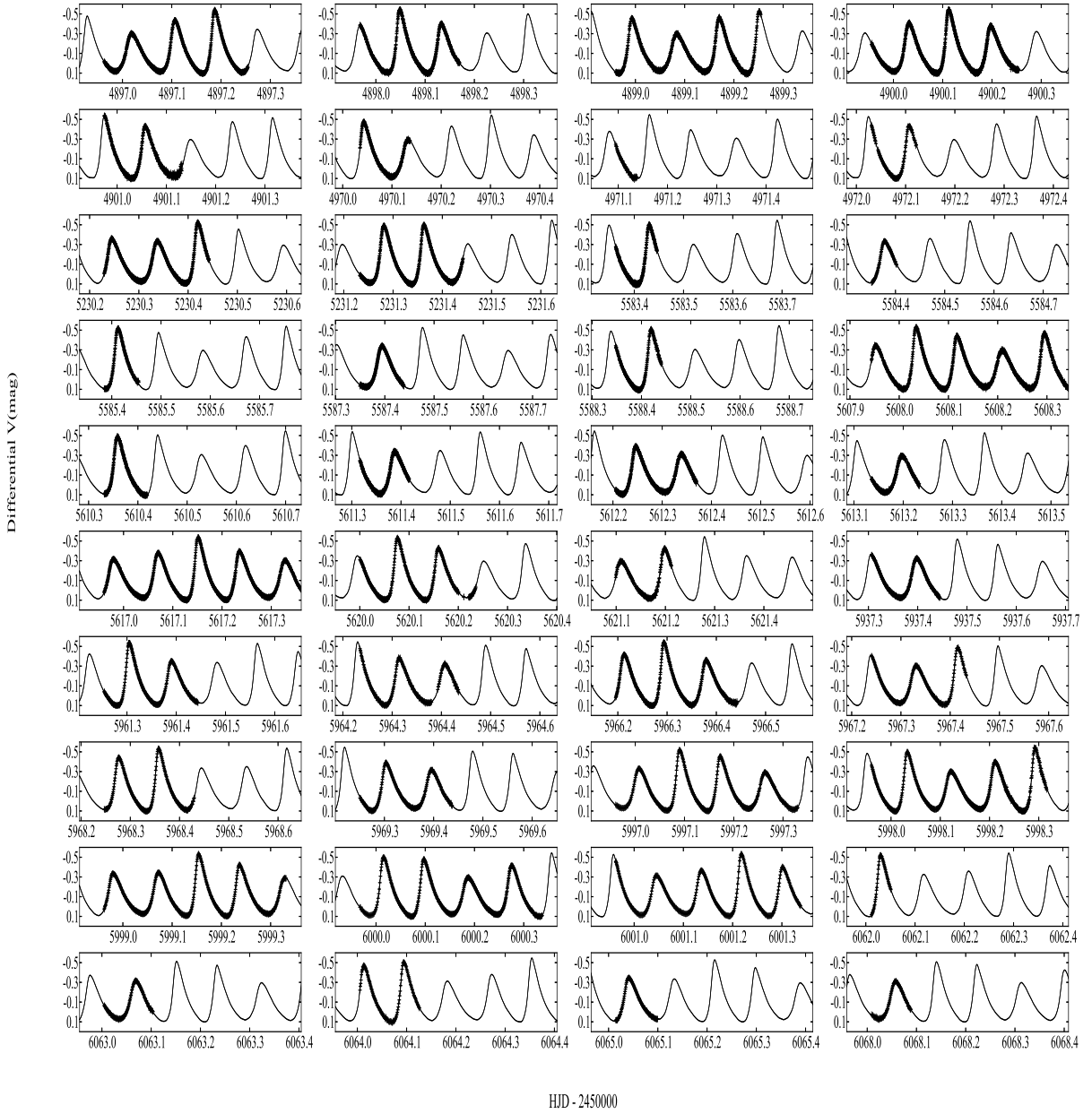


Fig. 2.— Light curves of AE UMa relative to the comparison star in the V band from 2009 to 2012, observed with the 85-cm telescope. The solid curves represent the fitting with a solution up to 18 frequencies listed in Table 3.

Table 3: Multi-frequency Solutions of the Light Curves of AE UMa in V Band taken with the 85-cm telescope in 2009 to 2012

NO.	Decomposition	2009			2010			2011			2012		
		Fre	Amp	S/N	Fre	Amp	S/N	Fre	Amp	S/N	Fre	Amp	S/N
1	f_0	11.62525	220.45	834.4	11.62944	216.36	5926.6	11.62549	218.93	1173.6	11.62558	218.26	1471.1
2	$2f_0$	23.25014	74.36	298.5	23.25888	73.25	1398.9	23.25036	73.77	522.5	23.25108	73.57	442.5
3	f_1	15.03109	45.29	158.3	15.01105	43.95	540.5	15.03201	45.00	404.0	15.03117	45.11	335.0
4	$3f_0$	34.87873	28.48	99.3	34.88832	29.66	1644.2	34.87620	27.70	104.7	34.87680	27.99	334.8
5	$f_0 + f_1$	26.65847	29.39	125.2	26.64049	28.76	342.4	26.65620	29.27	286.5	26.65665	29.72	192.6
6	$f_1 - f_0$	3.40580	25.47	195.5	3.42285	27.36	9794.9	3.40660	24.36	136.6	3.40572	25.44	160.5
7	$2f_0 + f_1$	38.28217	16.24	79.7	39.34215	15.07	174.1	38.28280	16.11	107.7	38.28216	15.97	129.1
8	$4f_0$	46.51274	12.80	60.1	46.55900	13.02	246.4	46.50160	12.91	126.4	46.50233	12.99	83.0
9	$3f_0 + f_1$	49.90705	9.31	57.0	49.94062	10.26	41.6	49.90820	9.14	71.3	49.90796	9.11	94.0
10	$5f_0$	58.13493	6.23	26.1	57.15747	4.19	29.6	58.12700	5.89	26.3	58.12768	5.99	40.7
11	$2f_0 - f_1$	8.22789	6.16	43.8	9.15509	6.12	418.7	8.22257	6.44	31.8	8.21896	6.21	32.2
12	$4f_0 + f_1$	61.54123	4.99	23.3	60.33288	5.85	89.9	61.53360	5.15	43.9	61.53427	4.92	39.2
13	$f_0 + 2f_1$	41.70315	4.33	21.0	41.77526	3.15	30.3	41.68940	4.16	25.6	41.68853	4.22	34.6
14	$2f_1$	30.08096	3.77	31.9	30.06334	5.03	128.5	30.06400	3.32	34.4	30.06174	4.00	32.0
15	$6f_0$	69.76912	3.68	21.8	69.85913	3.51	15.5	69.75240	3.74	31.7	69.75322	3.29	35.6
16	$2f_1 - f_0$	19.81409	3.45	16.4	18.22771	3.46	32.6	19.84420	3.04	2—	19.84574	3.16	18.1
17	$5f_0 + f_1$	73.16342	3.27	23.9	74.23048	3.31	10.1	73.15900	3.31	23.4	73.15980	3.42	38.0
18	$6f_0 + f_1$	84.76312	2.15	21.0	84.77368	2.83	72.5	84.78267	2.21	17.2	84.78566	2.19	25.1
19	$2f_0 + 2f_1$	53.34933	2.07	10.3	53.69338	1.82	13.3	53.31480	1.66	7.6	53.31282	2.26	23.9
20	$7f_0$	81.39280	2.00	9.4	80.56729	1.80	33.4	81.37984	1.90	14.2	81.38032	1.93	16.0
21	$7f_0 + f_1$	96.39730	1.45	14.2	96.36188	1.51	4.7	96.40807	1.60	16.5	96.41120	1.62	13.6
22	$3f_0 + 2f_1$	64.93553	1.60	7.7	63.83821	3.22	99.3	64.94397	1.64	15.7	64.93835	1.59	13.1
23	$4f_0 - f_1$	31.44828	1.76	9.5	31.54795	1.18	37.5	32.24212	1.34	6.4	31.47003	1.56	13.8
24	$2f_1 - 2f_0$	6.77661	1.41	15.8	7.79420	3.97	257.4	6.02561	2.05	9.0	7.78861	1.07	5.5
25	$2f_1 - f_0$	18.45877	1.40	5.5	18.22771	3.46	32.6	18.44237	2.04	13.0	18.43745	1.93	13.9
26	$4f_0 + 2f_1$	76.54723	1.32	14.9	—	—	—	75.79889	1.16	7.0	76.56296	1.18	9.4
27	$8f_0 + f_1$	108.00750	1.06	14.6	109.10478	1.26	9.7	108.03347	1.25	9.9	108.03549	0.99	9.9
28	$8f_0$	93.03898	1.22	7.2	—	—	—	93.01278	0.88	4.7	93.00586	1.18	10.2
29	$5f_0 + 2f_1$	88.20540	1.05	8.4	—	—	—	88.18550	1.06	8.4	88.18975	1.05	12.7
30	$6f_0 - f_1$	54.69265	1.20	7.9	—	—	—	53.31480	1.66	7.6	54.72485	0.98	7.7
31	$3f_1$	44.05397	1.03	4.2	—	—	—	43.09877	1.13	8.2	43.09681	1.00	9.3
32	$10f_0 + f_1$	131.28786	0.91	4.1	—	—	—	—	—	—	—	—	—
33	$9f_0 + f_1$	119.62969	0.82	5.4	118.71350	0.97	10.7	119.65510	0.72	5.3	118.65564	0.57	5.4
34	$6f_0 + 2f_1$	100.82309	0.78	5.2	100.77447	0.99	12.4	99.81467	1.01	5.4	99.81528	0.77	7.2
35	$7f_0 + 2f_1$	110.50225	0.73	4.7	110.99541	0.78	4.8	111.43957	0.69	7.3	—	—	—
36	$9f_0$	103.66567	0.71	6.4	104.89839	0.90	7.2	104.86428	0.69	6.1	103.65346	0.67	6.0
37	$8f_0 + 2f_1$	—	—	—	—	—	—	—	—	—	123.06760	0.54	4.7

Table 3: Multiple frequencies from the new data. Fre: Frequency in $c d^{-1}$. Amp: Amplitude in mmg .

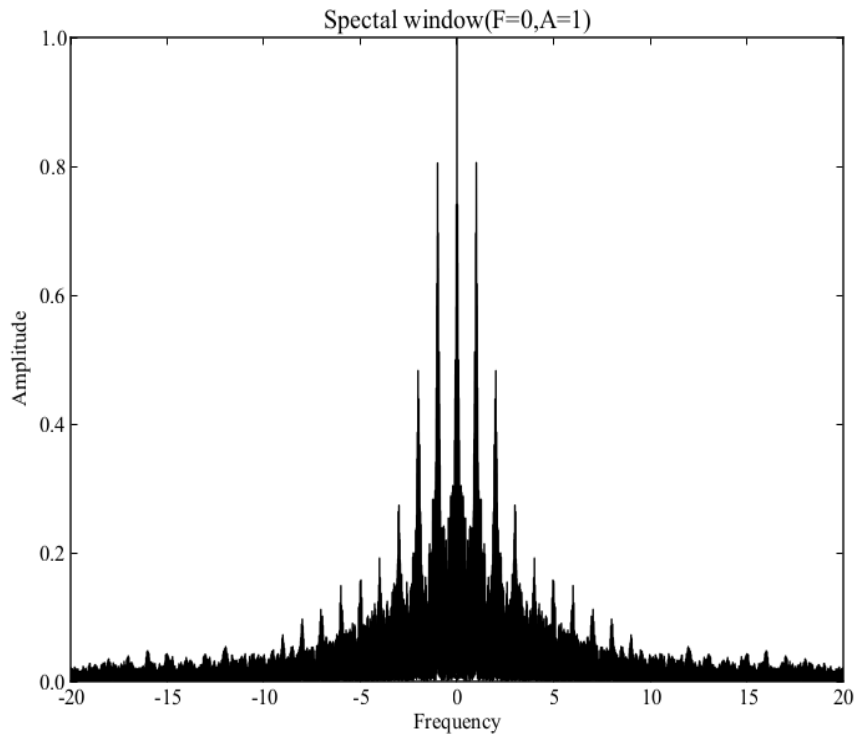


Fig. 3.— Spectral windows of the light curves in V for AE UMa in 2009 with the 85 cm telescope of NAOC.

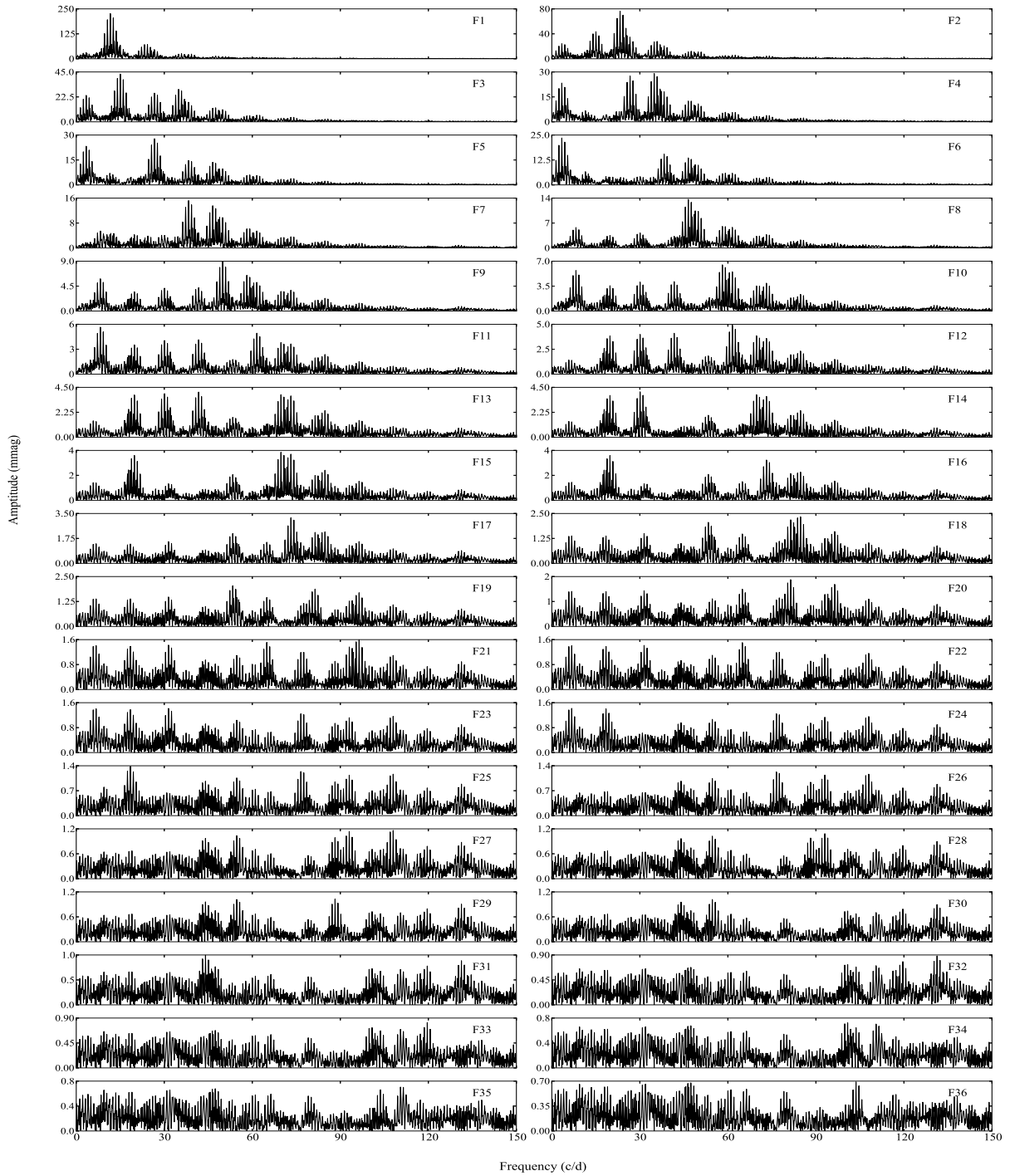


Fig. 4.— Amplitude spectra of the light curves of V for AE UMa collected in 2009 with the 85 cm telescope at Xinglong station of NAOC, and the frequency pre-whitening process. Note that the y-axis scales are optimized concerning the height of the high peaks in the panels.

1974 to 2001. By dividing the data into four segments of datasets, Zhou (2001) analyzed the pulsations of AE UMa. In Table 4, we listed the pulsation parameters of the fundamental and first overtone frequencies of AE UMa we obtained with those from Zhou (2001).

Table 4: Frequencies and amplitudes of AE UMa for different segments of observations

Years	f_0	f_1	A_{f_0}	A_{f_1}
1974-1977	11.62557	15.03097	216.9	34.1
1981-1987	11.62290	15.07259	219.6	29.4
1996-1998	11.62560	15.03122	210.9	36.8
2000-2001	11.62561	15.03119	207.0	38.6
2009-2012	11.62560	15.03123	219.0	45.1
Mean	11.62506	15.03944	214.7	36.8
σ	0.001078	0.016575	4.9	5.2

Table 4: The pulsation parameters of AE UMa from 1974 to 2012 from our results for 2009-2012 and Zhou (2001) for 1974-2001.

From Table 4, one finds that both the amplitudes and the frequencies were subject only to small changes, during a time base of 38 years. Considering the precision of the historical data, we nearly cannot get more conclusion about the variation of the frequencies using this method. But for amplitude, we can see that A_0 is stable and A_1 increasing with slight rate during the last 30 years.

4. The $O - C$ Diagram

With the new observations from 2009 to 2012, the light curves around the maxima were fitted with a third polynomial, which is sufficient to derive times of maximum light. 84 times of maximum light in V band were determined.

In order to make the $O - C$ analysis for the period change of AE UMa, we combined the maximum times newly determined with those provided by Agerer et al. (1999a), Pócs & Szeidl (2001), Pejcha et al. (2001), Zhou (2001), Agerer & Hubscher (2003), Hubscher (2005), Hubscher et al. (2005), Klingenberg et al. (2006), Hubscher et al. (2006), Hubscher & Walter (2007), Samolyk (2010), Hubscher (2007), Hubscher et al. (2009), Hubscher et al. (2010) and Huebscher & Monninger (2011). In total, 462 times of maximum light were collected and listed in Table 5. However, due to the low precisions of the data observed with either the photograph (pg) and visuel (vis), we discarded those times of maximum light and used the left 444 data points to make the $O - C$ analysis. The used linear ephemeris formula is,

$$HJD_{max} = 2442062.5824 + 0^d.08601707E \quad (2)$$

, which is given by Pócs & Szeidl (2001). The $O - C$ values are listed in Table 5. The $O - C$ diagram is shown in Figure 5. A straight-line fit to the 444 times of light maxima yields the ephemeris formula,

$$HJD_{max} = 2442062.5818(0) + 0.086017078(1)E \quad (3)$$

, with a standard deviation of $\sigma = 0.0024(5)$ *days*.

Table 5. Times of Maximum Light and $O - C$ values of AE UMa. T_{max} is the observed times of maximum light in $HJD - 2400000$. E : Cycle number. $O - C$ is in days. Det:detector. (pg=photograph, vis=visual, pe=photoelectric photometer.) S: source. Points not used in the $O - C$ analysis are marked with asterisk.

NO.	T_{max}	E	$O - C$	Det.	S	NO.	T_{max}	E	$O - C$	Det.	S
1	28632.398	-156133	-0.0510	pg	1*	26	42087.5263	290	0.0122	pe	4
2	31875.122	-118434	-0.0886	pg	2*	27	42087.6155	291	0.0154	pe	4
3	33379.256	-100948	-0.0509	pg	2*	28	42095.5298	383	0.0161	pe	3
4	35601.188	-75117	-0.0287	pg	2*	29	42095.6123	384	0.0126	pe	3
5	35604.337	-75080	-0.0623	vis	1*	30	42103.3513	474	0.0101	pe	4
6	35607.173	-75047	-0.0649	pg	2*	31	42106.4523	510	0.0145	pe	3
7	35981.202	-70699	-0.0385	pg	2*	32	42119.5252	662	0.0128	pe	3
8	38106.402	-45992	-0.0650	vis	1*	33	42121.5025	685	0.0117	pe	3
9	41059.368	-11662	-0.0687	vis	1*	34	42122.3628	695	0.0118	pe	4
10	41773.223	-3363	-0.0702	vis	1*	35	42122.4484	696	0.0114	pe	4
11	42062.5832	0	0.0141	pe	3	36	42128.2968	764	0.0106	pe	3
12	42065.5959	35	0.0162	pe	4	37	42128.3872	765	0.0150	pe	3
13	42065.6778	36	0.0121	pe	4	38	42128.4727	766	0.0145	pe	3
14	42068.3432	67	0.0110	pe	4	39	42128.5557	767	0.0114	pe	3
15	42068.4302	68	0.0120	pe	4	40	42133.4627	824	0.0155	pe	3
16	42068.5203	69	0.0160	pe	4	41	42133.5442	825	0.0110	pe	3
17	42068.6029	70	0.0126	pe	4	42	42134.4055	835	0.0121	pe	3
18	42068.6871	71	0.0108	pe	4	43	42147.3933	986	0.0113	pe	3
19	42069.3808	79	0.0164	pe	4	44	42148.4295	998	0.0153	pe	3
20	42069.4651	80	0.0147	pe	4	45	42148.5117	999	0.0115	pe	3
21	42069.5473	81	0.0108	pe	4	46	42159.4365	1126	0.0121	pe	3
22	42069.6363	82	0.0138	pe	4	47	42161.4145	1149	0.0117	pe	3
23	42086.4965	278	0.0146	pe	4	48	42453.5306	4545	0.0135	pe	3
24	42086.5787	279	0.0108	pe	4	49	42453.6137	4546	0.0105	pe	3
25	42087.4390	289	0.0110	pe	4	50	42460.4989	4626	0.0144	pe	3

Table 5—Continued

NO.	T_{max}	E	$O - C$	Det.	S	NO.	T_{max}	E	$O - C$	Det.	S
51	42532.407	5462	0.0121	vis	5*	76	46468.4601	51221	0.0052	pe	3
52	42830.6280	8929	0.0115	pe	3	77	46468.5468	51222	0.0059	pe	3
53	42837.5120	9009	0.0142	pe	3	78	46855.6279	55722	0.0097	pe	8
54	42838.4591	9020	0.0151	pe	3	79	46856.5729	55733	0.0085	pe	8
55	42866.496	9346	0.0104	vis	5*	80	46856.6561	55734	0.0057	pe	8
56	42869.3377	9379	0.0135	pe	3	81	46857.6017	55745	0.0051	pe	8
57	42869.4205	9380	0.0103	pe	3	82	46857.6925	55746	0.0099	pe	8
58	43162.5708	12788	0.0141	pe	3	83	46858.6382	55757	0.0094	pe	8
59	44633.4626	29888	0.0121	pe	3	84	46859.6666	55769	0.0056	pe	8
60	44633.5440	29889	0.0075	pe	3	85	46878.4181	55987	0.0053	pe	8
61	44633.6309	29890	0.0084	pe	3	86	46878.5064	55988	0.0076	pe	8
62	44634.4046	29899	0.0079	pe	3	87	46878.5946	55989	0.0098	pe	8
63	44634.4902	29900	0.0075	pe	3	88	46884.5262	56058	0.0062	pe	8
64	44634.5810	29901	0.0123	pe	3	89	46884.6117	56059	0.0057	pe	8
65	44692.4709	30574	0.0126	pe	3	90	46886.5907	56082	0.0063	pe	8
66	44696.343	30619	0.0140	vis	6*	91	48683.317	7697	0.0058	vis	9*
67	44696.426	30620	0.0110	vis	6*	92	50151.4564	94038	0.0040	pe	3
68	44696.520	30621	0.0189	vis	6*	93	50151.5384	94039	0.0000	pe	3
69	45355.4902	38282	0.0115	pe	3	94	50152.3170	94048	0.0044	pe	3
70	45355.5727	38283	0.0080	pe	3	95	50152.4862	94050	0.0016	pe	3
71	45382.3228	38594	0.0068	pe	3	96	50152.5756	94051	0.0050	pe	3
72	45382.4104	38595	0.0084	pe	3	97	50458.8815	97612	0.0037	CCD	10
73	45382.4997	38596	0.0116	pe	3	98	50458.9636	97613	-0.0001	CCD	10
74	45382.5807	38597	0.0066	pe	3	99	50459.8240	97623	0.0000	CCD	10
75	46114.332	47104	0.0098	vis	7*	100	50459.9113	97624	0.0013	CCD	10

Table 5—Continued

NO.	T_{max}	E	$O - C$	Det.	S	NO.	T_{max}	E	$O - C$	Det.	S
101	50467.7388	97715	0.0012	CCD	10	126	50902.2976	102767	0.0012	pe	3
102	50467.8236	97716	0.0000	CCD	10	127	50902.3819	102768	-0.0004	pe	3
103	50490.3607	97978	0.0006	pe	3	128	50903.3321	102779	0.0035	pe	3
104	50505.6697	98156	-0.0013	CCD	10	129	50903.4192	102780	0.0046	pe	3
105	50505.7595	98157	0.0023	CCD	10	130	50903.5009	102781	0.0003	pe	3
106	50505.8461	98158	0.0029	CCD	10	131	51269.5080	107036	0.0043	CCD	13
107	50516.7676	98285	0.0002	CCD	10	132	51283.4410	107198	0.0025	CCD	13
108	50554.4432	98723	0.0003	pe	3	133	51283.5250	107199	0.0005	CCD	13
109	50813.3550	101733	0.0004	pe	3	134	51283.6090	107200	-0.0014	CCD	13
110	50813.4408	101734	0.0002	pe	3	135	51318.3630	107604	0.0016	CCD	13
111	50813.6151	101736	0.0025	pe	3	136	51318.4460	107605	-0.0014	CCD	13
112	50813.6985	101737	-0.0001	pe	3	137	51608.0716	110972	0.0043	CCD	14
113	50848.4540	102141	0.0044	pe	3	138	51608.1577	110973	0.0044	CCD	14
114	50848.5391	102142	0.0035	pe	3	139	51608.2395	110974	0.0002	CCD	14
115	50848.6212	102143	-0.0003	pe	3	140	51608.3264	110975	0.0011	CCD	14
116	50849.4815	102153	-0.0002	pe	3	141	51609.0186	110983	0.0051	CCD	14
117	50849.5688	102154	0.0010	pe	3	142	51609.1006	110984	0.0011	CCD	14
118	50862.3840	102303	-0.0003	pe	11	143	51609.1865	110985	0.0010	CCD	14
119	50862.3840	102303	-0.0003	CCD	13	144	51609.2770	110986	0.0055	CCD	14
120	50872.2809	102418	0.0045	pe	3	145	51609.3583	110987	0.0008	CCD	14
121	50872.3634	102419	0.0010	pe	3	146	51610.0450	110995	-0.0006	CCD	14
122	50872.4481	102420	-0.0002	pe	3	147	51610.9969	111006	0.0050	CCD	14
123	50872.5394	102421	0.0050	pe	3	148	51611.0821	111007	0.0042	CCD	14
124	50899.3729	102733	0.0011	pe	3	149	51611.1627	111008	-0.0011	CCD	14
125	50899.4570	102734	-0.0007	pe	3	150	51612.0246	111018	0.0005	CCD	14

Table 5—Continued

NO.	T_{max}	E	$O - C$	Det.	S	NO.	T_{max}	E	$O - C$	Det.	S
151	51612.1091	111019	-0.0009	CCD	14	176	51941.2979	114846	0.0001	CCD	14
152	51612.2010	111020	0.0049	CCD	14	177	51941.3881	114847	0.0042	CCD	14
153	51612.2846	111021	0.0025	CCD	14	178	51942.1562	114856	-0.0017	CCD	14
154	51612.3704	111022	0.0022	CCD	14	179	51942.2473	114857	0.0033	CCD	14
155	51612.9692	111029	-0.0010	CCD	14	180	51942.3311	114858	0.0011	CCD	14
156	51613.0609	111030	0.0046	CCD	14	181	51942.4141	114859	-0.0019	CCD	14
157	51613.1453	111031	0.0030	CCD	14	182	52321.4089	119265	0.0012	CCD	15
158	51613.2276	111032	-0.0006	CCD	14	183	52371.3836	119846	-0.0000	CCD	15
159	51613.3156	111033	0.0013	CCD	14	184	52685.3460	123496	-0.0003	CCD	15
160	51615.0341	111053	-0.0005	CCD	14	185	52685.4369	123497	0.0045	CCD	15
161	51615.1260	111054	0.0053	CCD	14	186	52730.4187	124020	-0.0006	CCD	15
162	51615.2098	111055	0.0031	CCD	14	187	52739.3617	124124	-0.0034	CCD	15
163	51615.2919	111056	-0.0007	CCD	14	188	52745.4702	124195	-0.0021	CCD	16
164	51615.9855	111064	0.0046	CCD	14	189	52980.5608	126928	0.0034	CCD	17
165	51616.0705	111065	0.0036	CCD	14	190	52980.6421	126929	-0.0012	CCD	17
166	51616.1526	111066	-0.0002	CCD	14	191	52980.7279	126930	-0.0014	CCD	17
167	51616.2388	111067	-0.0000	CCD	14	192	53003.5231	127195	-0.0008	CCD	16
168	51929.2556	114706	0.0002	CCD	14	193	53028.2942	127483	-0.0026	CCD	16
169	51929.3464	114707	0.0050	CCD	14	194	53028.3871	127484	0.0042	CCD	16
170	51930.2059	114717	0.0043	CCD	14	195	53028.4705	127485	0.0016	CCD	16
171	51930.2885	114718	0.0009	CCD	14	196	53028.5522	127486	-0.0027	CCD	16
172	51930.3721	114719	-0.0015	CCD	14	197	53028.6420	127487	0.0010	CCD	16
173	51931.2316	114729	-0.0021	CCD	14	198	53069.4119	127961	-0.0011	CCD	16
174	51931.3203	114730	0.0005	CCD	14	199	53069.5029	127962	0.0038	CCD	16
175	51941.2102	114845	-0.0015	CCD	14	200	53070.4493	127973	0.0040	CCD	16

Table 5—Continued

NO.	T_{max}	E	$O - C$	Det.	S	NO.	T_{max}	E	$O - C$	Det.	S
201	53070.5320	127974	0.0007	CCD	16	226	54079.8580	139708	0.0011	CCD	21
202	53090.4053	128205	0.0040	CCD	16	227	54079.9437	139709	0.0008	CCD	21
203	53094.3575	128251	-0.0005	CCD	16	228	54102.6471	139973	-0.0043	CCD	21
204	53110.3619	128437	0.0046	CCD	19	229	54102.7365	139974	-0.0009	CCD	21
205	53409.5286	131915	0.0036	CCD	18	230	54102.8254	139975	0.0019	CCD	21
206	53409.6108	131916	-0.0002	CCD	18	231	54103.6849	139985	0.0012	CCD	21
207	53409.6941	131917	-0.0029	CCD	18	232	54103.7677	139986	-0.0019	CCD	21
208	53427.3272	132122	-0.0033	CCD	19	233	54104.7117	139997	-0.0041	CCD	21
209	53427.4181	132123	0.0015	CCD	19	234	54107.6358	140031	-0.0046	CCD	21
210	53427.5031	132124	0.0005	CCD	19	235	54107.7251	140032	-0.0013	CCD	21
211	53451.4136	132402	-0.0017	CCD	17	236	54107.8138	140033	0.0013	CCD	21
212	53451.5042	132403	0.0028	CCD	17	237	54107.8944	140034	-0.0040	CCD	21
213	53484.3616	132785	0.0016	CCD	17	238	54110.7388	140067	0.0017	CCD	21
214	53765.3803	136052	0.0022	CCD	20	239	54110.8207	140068	-0.0023	CCD	21
215	53765.4660	136053	0.0019	CCD	20	240	54110.9051	140069	-0.0039	CCD	21
216	53765.5462	136054	-0.0038	CCD	20	241	54110.9977	140070	0.0026	CCD	21
217	53766.3278	136063	0.0035	CCD	20	242	54125.7056	140241	0.0015	CCD	21
218	53766.4079	136064	-0.0023	CCD	20	243	54125.7883	140242	-0.0017	CCD	21
219	53766.4943	136065	-0.0019	CCD	20	244	54125.8716	140243	-0.0044	CCD	21
220	53766.5849	136066	0.0026	CCD	20	245	54125.9649	140244	0.0028	CCD	21
221	53794.3619	136389	-0.0039	CCD	18	246	54131.5550	140309	0.0018	CCD	21
222	53795.3115	136400	-0.0005	CCD	18	247	54131.6392	140310	0.0000	CCD	21
223	53795.3998	136401	0.0017	CCD	18	248	54131.7212	140311	-0.0040	CCD	21
224	53827.6570	136776	0.0025	CCD	18	249	54131.8106	140312	-0.0006	CCD	21
225	54079.7666	139707	-0.0042	CCD	21	250	54131.8989	140313	0.0016	CCD	21

Table 5—Continued

NO.	T_{max}	E	$O - C$	Det.	S	NO.	T_{max}	E	$O - C$	Det.	S
251	54136.5446	140367	0.0024	CCD	21	276	54197.4402	141075	-0.0021	CCD	22
252	54136.6275	140368	-0.0006	CCD	21	277	54198.3850	141086	-0.0035	CCD	22
253	54136.7104	140369	-0.0038	CCD	21	278	54198.4741	141087	-0.0004	CCD	22
254	54136.7998	140370	-0.0004	CCD	21	279	54202.4288	141133	-0.0025	CCD	22
255	54136.8882	140371	0.0019	CCD	21	280	54414.8939	143603	0.0001	CCD	21
256	54136.9697	140372	-0.0025	CCD	21	281	54414.9804	143604	0.0006	CCD	21
257	54137.6581	140380	-0.0022	CCD	21	282	54417.7271	143636	-0.0052	CCD	21
258	54137.7491	140381	0.0026	CCD	21	283	54417.9058	143638	0.0014	CCD	21
259	54137.8311	140382	-0.0013	CCD	21	284	54417.9856	143639	-0.0047	CCD	21
260	54139.7226	140404	-0.0022	CCD	21	285	54440.6958	143903	-0.0031	CCD	21
261	54139.8124	140405	0.0015	CCD	21	286	54442.7619	143927	-0.0014	CCD	21
262	54139.8942	140406	-0.0026	CCD	21	287	54442.8516	143928	0.0022	CCD	21
263	54141.7876	140428	-0.0016	CCD	21	288	54442.9342	143929	-0.0011	CCD	21
264	54141.8768	140429	0.0015	CCD	21	289	54451.6243	144030	0.0012	CCD	21
265	54141.9575	140430	-0.0037	CCD	21	290	54460.6513	144135	-0.0035	CCD	21
266	54152.6241	140554	-0.0032	CCD	21	291	54460.7433	144136	0.0023	CCD	21
267	54153.5746	140565	0.0010	CCD	21	292	54460.8247	144137	-0.0022	CCD	21
268	54154.6883	140578	-0.0034	CCD	21	293	54460.9089	144138	-0.0040	CCD	21
269	54154.7800	140579	0.0021	CCD	21	294	54467.7955	144218	0.0011	CCD	21
270	54154.8618	140580	-0.0020	CCD	21	295	54468.7392	144229	-0.0013	CCD	21
271	54171.4664	140773	0.0012	CCD	22	296	54468.8220	144230	-0.0045	CCD	21
272	54174.4816	140808	0.0058	CCD	22	297	54468.9120	144231	-0.0005	CCD	21
273	54175.4206	140819	-0.0013	CCD	22	298	54469.6815	144240	-0.0052	CCD	21
274	54196.4976	141064	0.0014	CCD	22	299	54469.7701	144241	-0.0026	CCD	21
275	54197.3590	141074	0.0026	CCD	22	300	54469.8603	144242	0.0015	CCD	21

Table 5—Continued

NO.	T_{max}	E	$O - C$	Det.	S	NO.	T_{max}	E	$O - C$	Det.	S
301	54469.9414	144243	-0.0033	CCD	21	326	54837.6637	148518	-0.0044	CCD	21
302	54506.5887	144669	0.0006	CCD	23	327	54837.7565	148519	0.0022	CCD	21
303	54512.5199	144738	-0.0033	CCD	23	328	54843.6886	148588	-0.0007	CCD	21
304	54513.4650	144749	-0.0044	CCD	23	329	54843.7704	148589	-0.0050	CCD	21
305	54513.5559	144750	0.0004	CCD	23	330	54843.8567	148590	-0.0047	CCD	21
306	54524.4815	144877	0.0018	CCD	23	331	54843.9494	148591	0.0019	CCD	21
307	54769.8859	147730	-0.0007	CCD	21	332	54846.6137	148622	-0.0002	CCD	21
308	54770.8336	147741	0.0007	CCD	21	333	54846.6960	148623	-0.0039	CCD	21
309	54770.9152	147742	-0.0036	CCD	21	334	54847.7336	148635	0.0014	CCD	21
310	54781.8384	147869	-0.0046	CCD	21	335	54847.8164	148636	-0.0018	CCD	21
311	54781.9301	147870	0.0010	CCD	21	336	54847.8988	148637	-0.0054	CCD	21
312	54788.8080	147950	-0.0024	CCD	21	337	54855.6469	148727	0.0011	CCD	21
313	54788.8912	147951	-0.0052	CCD	21	338	54855.7316	148728	-0.0001	CCD	21
314	54788.9833	147952	0.0008	CCD	21	339	54855.8119	148729	-0.0059	CCD	21
315	54791.7333	147984	-0.0017	CCD	21	340	54855.9023	148730	-0.0015	CCD	21
316	54791.8157	147985	-0.0053	CCD	21	341	54864.5873	148831	-0.0042	CCD	21
317	54791.9080	147986	0.0009	CCD	21	342	54864.6724	148832	-0.0051	CCD	21
318	54791.9938	147987	0.0007	CCD	21	343	54864.7649	148833	0.0013	CCD	21
319	54807.8222	148171	0.0019	CCD	21	344	54864.8477	148834	-0.0019	CCD	21
320	54807.9032	148172	-0.0030	CCD	21	345	54864.9296	148835	-0.0060	CCD	21
321	54807.9866	148173	-0.0056	CCD	21	346	54868.6346	148878	0.0002	CCD	21
322	54816.6793	148274	-0.0006	CCD	21	347	54868.7166	148879	-0.0037	CCD	21
323	54816.7612	148275	-0.0048	CCD	21	348	54868.8033	148880	-0.0031	CCD	21
324	54816.8501	148276	-0.0019	CCD	21	349	54868.8941	148881	0.0016	CCD	21
325	54816.9399	148277	0.0018	CCD	21	350	54878.6935	148995	-0.0048	CCD	21

Table 5—Continued

NO.	T_{max}	E	$O - C$	Det.	S	NO.	T_{max}	E	$O - C$	Det.	S
351	54878.7811	148996	-0.0032	CCD	21	376	54912.4146	149387	-0.0025	CCD	24
352	54878.8721	148997	0.0016	CCD	21	377	54924.3742	149526	0.0006	CCD	24
353	54894.4412	149178	0.0016	CCD	24	378	54970.0431	150057	-0.0055	CCD	26
354	54894.5227	149179	-0.0028	CCD	24	379	54972.1078	150081	-0.0052	CCD	26
355	54894.6071	149180	-0.0044	CCD	24	380	55230.2455	153082	-0.0050	CCD	26
356	54897.0188	149208	-0.0012	CCD	26	381	55230.3379	153083	0.0012	CCD	26
357	54897.1069	149209	0.0008	CCD	26	382	55230.4201	153084	-0.0025	CCD	26
358	54897.1883	149210	-0.0037	CCD	26	383	55231.2818	153094	-0.0009	CCD	26
359	54898.0490	149220	-0.0032	CCD	26	384	55231.3635	153095	-0.0053	CCD	26
360	54898.1331	149221	-0.0051	CCD	26	385	55259.4108	153421	0.0003	CCD	25
361	54898.3084	149223	-0.0018	CCD	24	386	55293.3826	153816	-0.0045	CCD	25
362	54898.9931	149231	-0.0053	CCD	26	387	55293.4752	153817	0.0019	CCD	25
363	54899.0837	149232	-0.0007	CCD	26	388	55302.3318	153920	-0.0011	CCD	25
364	54899.1706	149233	0.0001	CCD	26	389	55303.3591	153932	-0.0060	CCD	25
365	54900.0318	149243	0.0011	CCD	26	390	55304.3959	153944	-0.0014	CCD	25
366	54900.1129	149244	-0.0037	CCD	26	391	55304.4775	153945	-0.0059	CCD	25
367	54900.1978	149245	-0.0048	CCD	26	392	55305.3388	153955	-0.0047	CCD	25
368	54901.0576	149255	-0.0052	CCD	26	393	55305.4238	153956	-0.0057	CCD	25
369	54904.4199	149294	0.0023	CCD	24	394	55309.3848	154002	-0.0015	CCD	25
370	54904.5006	149295	-0.0029	CCD	24	395	55310.4124	154014	-0.0061	CCD	25
371	54909.3147	149351	-0.0057	CCD	24	396	55311.3662	154025	0.0014	CCD	25
372	54909.4087	149352	0.0021	CCD	24	397	55311.4488	154026	-0.0020	CCD	25
373	54909.4895	149353	-0.0030	CCD	24	398	55583.4313	157188	-0.0058	CCD	26
374	54910.4335	149364	-0.0052	CCD	24	399	55584.3787	157199	-0.0046	CCD	26
375	54912.3323	149386	0.0012	CCD	24	400	55585.4132	157211	-0.0023	CCD	26

Table 5—Continued

NO.	T_{max}	E	$O - C$	Det.	S	NO.	T_{max}	E	$O - C$	Det.	S
401	55587.3946	157234	0.0006	CCD	26	426	55964.3148	161616	-0.0063	CCD	26
402	55588.4201	157246	-0.0060	CCD	26	427	55964.4073	161617	0.0001	CCD	26
403	55607.9528	157473	0.0007	CCD	26	428	55966.2133	161638	-0.0002	CCD	26
404	55608.0348	157474	-0.0032	CCD	26	429	55966.2942	161639	-0.0053	CCD	26
405	55608.1180	157475	-0.0060	CCD	26	430	55966.3797	161640	-0.0058	CCD	26
406	55608.2099	157476	-0.0001	CCD	26	431	55967.3311	161651	-0.0006	CCD	26
407	55608.2953	157477	-0.0007	CCD	26	432	55967.4159	161652	-0.0018	CCD	26
408	55608.3763	157478	-0.0057	CCD	26	433	55968.2773	161662	-0.0006	CCD	26
409	55610.3591	157501	-0.0013	CCD	26	434	55968.3582	161663	-0.0057	CCD	26
410	55611.3877	157513	-0.0049	CCD	26	435	55969.3038	161674	-0.0063	CCD	26
411	55612.2469	157523	-0.0059	CCD	26	436	55969.3959	161675	-0.0002	CCD	26
412	55612.3392	157524	0.0003	CCD	26	437	55997.0080	161996	0.0002	CCD	26
413	55613.1980	157534	-0.0010	CCD	26	438	55997.0906	161997	-0.0031	CCD	26
414	55616.9800	157578	-0.0038	CCD	26	439	55997.1730	161998	-0.0067	CCD	26
415	55617.0705	157579	0.0006	CCD	26	440	55997.2639	161999	-0.0018	CCD	26
416	55617.1520	157580	-0.0038	CCD	26	441	55998.0337	162008	-0.0062	CCD	26
417	55617.2358	157581	-0.0060	CCD	26	442	55998.1221	162009	-0.0038	CCD	26
418	55617.3281	157582	0.0002	CCD	26	443	55998.2119	162010	-0.0000	CCD	26
419	55620.0772	157614	-0.0032	CCD	26	444	55998.2927	162011	-0.0052	CCD	26
420	55620.1602	157615	-0.0062	CCD	26	445	55998.9808	162019	-0.0053	CCD	26
421	55621.1103	157626	-0.0023	CCD	26	446	55999.0727	162020	0.0005	CCD	26
422	55621.1986	157627	-0.0000	CCD	26	447	55999.1547	162021	-0.0034	CCD	26
423	55937.3981	161303	0.0002	CCD	26	448	55999.2375	162022	-0.0066	CCD	26
424	55961.3051	161581	-0.0054	CCD	26	449	56000.0161	162031	-0.0022	CCD	26
425	55961.3907	161582	-0.0058	CCD	26	450	56000.0978	162032	-0.0065	CCD	26

According for the evolution-origin continuous changes of period of AE UMa, we obtained a forced quadratic solution by using a second-order polynomial fit,

$$HJD_{max} = 2442062.5821(6) + 0.086017060(1)E + 0.5 \times 1.1(8) \times 10^{-13}E^2 \quad (4)$$

, with the standard deviation of $\sigma = 0.0024(4)$ *days*. According to this fomula, one gets the period change rate of AE UMa as $(1/P_0)(dP_0/dt) = 5.4(8) \times 10^{-9} \text{ yr}^{-1}$, which is different from the result provided by Zhou (2001) of $-0.35 \times 10^{-10} \text{ yr}^{-1}$. Hence, the fundamental period is increasing other than decreasing.

Due to the star's double mode pulsation nature, the observed times of maximum light used in the above $O - C$ diagram analysis are not the times of maximum light of the fundamental period, but the result of the combination of the two modes. However, as the amplitude of the fundamental frequency is much larger than that of the first overtone frequency, we consider that that the period changes of P_0 we get is reliability.

As can be seen in Table 3, the sixth frequency is the modulation frequency $f_m = f_1 - f_0$, which modulates the amplitude of the light curves.

Since the modulation frequency f_m has not varied significantly (Pócs & Szeidl (2001)), one may take the method which used in Pócs & Szeidl (2001) and Zhou (2001) to calculate the rate of changes of the first overtone frequency. By replacing the period in Eq. (2) with the modulation period $P_m = 0^d.0293616$, the fit with the times of maximum light leads to the study of its secular changes. The ephemeris is,

$$HJD_{max}(P_m) = 2442062.5890(3) + 0.293615846(8)E \quad (5)$$

with a standard deviation of $\sigma = 0.0859$ *days*. A second-order polynomial fit gives,

$$HJD_{max}(P_m) = 2442062.5806(3) + 0.293617291(4)E - 0.5 \times 2.98(12) \times 10^{-11}E^2 \quad (6)$$

with a standard deviation of $\sigma = 0.0857$ *days*. Thus one can get the period change of f_m is

Table 5—Continued

NO.	T_{max}	E	$O - C$	Det.	S	NO.	T_{max}	E	$O - C$	Det.	S
451	56000.1874	162033	-0.0029	CCD	26	457	56062.0312	162752	-0.0054	CCD	26
452	56000.2762	162034	-0.0001	CCD	26	458	56063.0691	162764	0.0002	CCD	26
453	56001.0459	162043	-0.0046	CCD	26	459	56064.0137	162775	-0.0013	CCD	26
454	56001.1368	162044	0.0002	CCD	26	460	56064.0948	162776	-0.0063	CCD	26
455	56001.2186	162045	-0.0039	CCD	26	461	56065.0419	162787	-0.0053	CCD	26
456	56001.3023	162046	-0.0062	CCD	26	462	56068.0580	162822	0.0001	CCD	26

Note. — Source: (1) Tsesevich (1973); (2) Filatov (1960); (3) Pócs & Szeidl (2001); (4) Broglia & Conconi (1975); (5) Braune et al. (1979); (6) Braune & Mundry (1982); (7) Huebscher et al. (1985); (8) Rodriguez et al. (1992); (9) Hübscher et al. (1992); (10) Hintz et al. (1997a); (11) Agerer et al. (1999b); (12) Agerer et al. (1999a); (13) Pejcha et al. (2001); (14) Zhou (2001); (15) Agerer & Hubscher (2003); (16) Hubscher (2005); (17) Hubscher et al. (2005); (18) Klingenberg et al. (2006); (19) Hubscher et al. (2006); (20) Hubscher & Walter (2007); (21) Samolyk (2010); (22) Hubscher (2007); (23) Hubscher et al. (2009); (24) Hubscher et al. (2010); (25) Huebscher & Monninger (2011); (26) this work.

$(1/P_m)(dP_m/dt) = -1.2(9) \times 10^{-7} \text{ yr}^{-1}$. From the relationship $f_1 = f_0 + f_m$, one derived

$$\frac{1}{P_1} \frac{dP_1}{dt} = P_1 \left(\frac{1}{P_m^2} \frac{dP_m}{dt} + \frac{1}{P_0^2} \frac{dP_0}{dt} \right). \quad (7)$$

Together with the value of $(1/dP_0)(dP_0/dt)$, one gets $(1/P_1)(dP_1/dt) = -2.8(4) \times 10^{-8} \text{ yr}^{-1}$.

This value agrees with $-7.3 \times 10^{-8} \text{ yr}^{-1}$ derived by Pócs & Szeidl (2001) and $-4.3 \times 10^{-8} \text{ yr}^{-1}$ derived by Zhou (2001) in the order of magnitude.

5. CONSTRAINTS FROM THE THEORETICAL MODELS

5.1. Physical Parameters

Rodriguez et al. (1992) made *wbyβ* photoelectric photometry for AE UMa. Intrinsic $b - y$, m_1 and c_1 values were derived and the physical parameters were determined. The effective temperature of AE UMa varied from $8130K$ at the light maximum to $7160K$ at the light minimum. When the secondary period is in phase with the fundamental period, the effective temperature can reach $8320K$. The surface gravity $\log g$ varied from 4.13 to 3.78. The mean values obtained along the cycle were $\langle T_{eff} \rangle = 7560K$ and $\langle \log g \rangle = 3.90$. The metal abundance was estimated from the δm_1 at the minimum light as $[Fe/H] = -0.3$. By using the $\log g - \log P$ relation derived by Claret et al. (1990), Rodriguez et al. (1992) obtained the values of $M = 1.80 M_\odot$, $Age = 1.3 \times 10^9 \text{ yr}$ and $M_{bol} = 1^m.76$. Hintz et al. (1997a) provided the value of $[Fe/H] = -0.1$ according to the relation between the P_1/P_0 ratio and the $[Fe/H]$ value for dwarf Cepheids which derived from Hintz et al. (1997b). They got the $[Fe/H]$ range from -0.4 to -0.1 . We listed the parameters of AE UMa from Rodriguez et al. (1992) and Hintz et al. (1997a) in Table 6.

Table 6: Physical parameters of AE UMa from Rodriguez et al. (1992) and Hintz et al. (1997a)

Parameters	Mean value	Intervals
$[Fe/H]$	-0.3	[-0.4,-0.1]
T_{eff}	7569	[7160,8320]
$\log g$	3.90	[3.78,4.16]
M_{bol}	—	[1.53,1.76]
M	—	[1.80,1.86]
$\log(L/L_{\odot})$	—	[1.196,1.288]
$\log T_{eff}$	—	[3.855,3.920]

Table 6: $\log(L/L_{\odot})$ value was derived base on $\log(L/L_{\odot}) = 0.4(M_{bol_{\odot}} - M_{bol})$.

5.2. Constraints from f_0 and f_1

Modules for Experiments in Stellar Astrophysics (MESA) is a suite of source-open, robust, efficient, thread-safe libraries for a wide range of applications in computational stellar astrophysics (Paxton et al. (2011, 2013)). A 1-D stellar evolution module, MESA star, combines many of the numerical and physics modules for simulations of a wide range of stellar evolution scenarios ranging from very-low mass to massive stars, including advanced evolutionary phases. The "astero" extension to MESA star implements an integrated approach that passes results automatically between MESA star and the new MESA module based on the adiabatic code ADIPLS (Christensen-Dalsgaard (2008)).

The κ module of MESA divides the opacity tables into a high-temperature domain, $\log(T/K) \geq 4$, and a low-temperature domain, $\log(T/K) \leq 4$. The exact range of $\log T$ over which the tables are blended can be adjusted at the runtime. Moreover, the κ module supports low- T opacities from either Ferguson et al. (2005) or Freedman et al. (2008) with updates to the molecular hydrogen pressure-induced opacity (Frommhold et al. (2010)) and the ammonia opacity (Yurchenko et al. (2011)). The electron conduction opacity tables,

based on Cassisi et al. (2007), have been expanded (Potekhin & Chabrier (2010)) to cover higher temperature (up to $10^{10}K$, originally 10^9K) and densities (up to $10^{11.5} g cm^{-3}$, originally $10^{9.75} g cm^{-3}$).

In the MESA version 4740, the astero extension enables calculation of selected pulsation frequencies by MESA star during the evolution of the model. This allows fitting to the observations that can include spectroscopic constraints (e.g., $[Fe/H]$ and T_{eff}), asteroseismic constraints, the large frequency separation ($\Delta\nu$) and the frequency of maximum power (ν_{max}), and even individual frequencies observed. For the automated χ^2 minimization, astero will evolve a pre-main sequence model from a user defined starting point, and find the best match along that single evolutionary track. The code then recalculates the track, again initiated at the pre-main sequence, with different initial parameters such as mass, composition, mixing length parameter and overshoot, and repeats until the lowest χ^2 has been found.

We used the scan-grid mode to minimize the χ^2 for each model, which helps to compact the intervals of the physical parameters. In all the calculations, the mixing-length parameter α_{MLT} was always chosen to be 1.89, since the choice has actually a very small effect on our models (Yang et al. (2012)). The convective overshooting parameter $f_{ov} = 0.015$ was the initial value of MESA. Table 7 lists the parameters of the grid of model to search for f_0 and f_1 of AE UMa.

The grid is shown in Table 7.

As the result, we got the models which included the frequencies f_0 and f_1 along with the stellar evolution tracks. Then, we chose the results whose $\chi^2 \leq 1$, and obtained the intervals of the parameters in Table 8.

One can see that the results were in agreement with the values in Rodriguez et al.

Table 7: The parameters of the grid of model to search for f_0 and f_1

Parameters	Maximum	Minimum	Step
$[Fe/H]$	-0.1	-0.4	0.05
initial Y	0.33	0.23	0.02
Mass	1.90	1.60	0.02

Table 7: The grid was constructed also within the parameter intervals of T_{eff} , $\log g$ and $\log(L/L_{\odot})$ as listed in Table 6.

Table 8: The parameters determined with the constraints from f_0 and f_1

Parameters	Maximum	Minimum
$[Fe/H]$	-0.2	-0.4
initial Y	0.27	0.23
Mass	1.88	1.68

Table 8: The grid was constructed also within the parameters intervals of T_{eff} , $\log g$ and $\log(L/L_{\odot})$ as listed in Table 6.

(1992), except the mass. With their observations and the method used, one can believe that the $[Fe/H]$ and the $\log g$ values were in great reliability (Strömberg (1956); Crawford & Mander (1966)). So, we decided to use the value $[Fe/H] = -0.3$ and $3.77 \leq \log g \leq 4.16$.

We used the formula

$$[Fe/H] = \log\left(\frac{Z}{X}\right) - \log\left(\frac{Z}{X}\right)_{\odot} \quad (8)$$

and the formula

$$X + Y + Z = 1 \quad (9)$$

to calculate the initial Z. In Girardi et al. (2000), the model was calculated with the couple of value $(Y, Z) = (0.25, 0.008)$, which accord with the values in our previous calculation (derived by MESA astero with the value of $[Fe/H]$).

At last, integrating all the information about the value of (Y, Z) , we decided to choose $(Y, Z) = (0.25, 0.008521)$ as the unique initial value for the subsequent calculation.

5.3. Constraints from the Period Variation

Not like the solar-like stars for which many frequencies are detected, HADS exits only one or two frequencies. As a result, the period variation becomes a very important constraint on the model calculation of these stars. Detection of high precision of period variation may offer strong constraints on AE UMa. It is interesting that AE UMa exits two frequencies with period variations in different scales and signs. But with the linear pulsation theory, variation of the period along with the stellar evolution should have values in the same sign and the same scale in most time. We used two different ways to calculate the period variations of AE UMa theoretically.

5.3.1. Calculation from Stellar Evolution Effect

The variation rate of the fundamental period derived from long intervals of observations of AE UMa shows a positive period change. From the theoretical point of view, the period changes caused by stellar evolution in and across the lower instability strip permit an observational test of stellar evolution theory (Breger & Pamyatnykh (1998)).

Assuming that the stellar mass $M = \text{constant}$ for the δ Scuti stars during the observation interval with mass of $1.68 - 1.88 M_{\odot}$ and that the variation of pulsation constant is negligible as a very small quantity, Breger & Pamyatnykh (1998) got

$$\frac{1}{P} \frac{dP}{dt} \approx -0.69 \frac{dM_{bol}}{dt} - \frac{3}{T_{eff}} \frac{dT_{eff}}{dt}. \quad (10)$$

where P is the period of a radial pulsation, M_{bol} is the bolometric absolute magnitude, T_{eff}

is the effective temperature.

As indicated by Rodríguez & Breger (2001), the SX Phe variables locate on or near the main sequence of the H-R diagram. Consequently, the evolutionary models are constructed from the pre-main-sequence Hayashi phase to the end of the post main sequence. As mentioned, the parameters we used are $(Y, Z) = (0.25, 0.008521)$, $\alpha_{MLT} = 1.89$ and $f_{ov} = 0.015$. In addition, we do not take the effect of rotation into account since AE UMa is a low-speed rotator.

The evolutionary tracks we constructed from $1.68 M_{\odot}$ to $1.88 M_{\odot}$ are shown in Figure 6, and the corresponding variation of the period were marked in the figure.

As shown in the Figure 6, the state which are consonant with the observed period change values derived from the $O - C$ analysis appear before the first turn-offs and after the second turn-offs on the evolutionary tracks when they leave the MS.

5.3.2. *Calculaiton from ADIPLS*

ADIPLS (the Aarhus adiabatic oscillation package) is a programme for calculation of adiabatic oscillations of stellar models (Christensen-Dalsgaard (2008)). We used it to calculate the frequencies of the model at each step of our evolutionary state. As a result, we got the frequencies of the model of f_0 and f_1 then deduced the variation of the frequencies of f_0 and f_1 . In the calculation, we assumed that f_0 and f_1 are the frequencies with $l = 0$ and $n = 1, 2$.

We calculated the evolutionary tracks from $1.68 M_{\odot}$ to $1.88 M_{\odot}$, getting the frequencies on each tracks, as shown in Figure 7.

In Figure 7, one can see that the models with appropriate frequencies for AE UMa

could appear (a) just before the first turn-offs, (b) after the first and before the second turn-offs, (c) just after the second turn-offs.

In addition, we also calculated the variation of the frequencies of the models using ADIPLS. The results are shown in Figure 8. It was not surprising that Figure 8 was in accord with Figure 6, which showed also the variation of the fundamental frequency.

In Figure 9, we show the models with variation of the first overtone frequency f_1 in accord with the observed values. For the adiabaticity of the code ADIPLS, we get the variation of f_1 almost as that of f_0 , with the same scale and the sign, even though they may not be equal to each other exactly in every points.

The $\log(L/L_\odot)$ values from literatures have a low reliability, but the $\log g$ values have a high reliability are not sensitive to the evolutionary effect. As a result, we show the figures both of them ($\log(L/L_\odot)$ vs $\log T_{eff}$, $\log g$ vs $\log T_{eff}$).

Integrating the results of calculation of the frequencies and the variation of frequencies and comparison with the observed values, we can conclude that AE UMa should locate on either before the first turn-offs or after the second turn-offs of the evolutionary tracks leaving the MS.

We assume that AE UMa is a regular radial pulsator with two frequencies. The variation of the fundamental frequency of AE UMa is caused by the evolutionary effect. The rate of the variation is consistant with the theoretically predicted values by Breger & Pamyatnykh (1998).

On the other hand, we would discuss the variation of the first overtone period which puts another constraint on the models. But once we put these constraints (f_0 , f_1 , $(1/P_0)(dP_0/dt)$ and $(1/P_1)(dP_1/dt)$) together, we cannot find any overlap on the evolutionary tracks (superimposing Figure 7, Figure 8 and Figure 9). Considering with the

adiabaticity of ADIPLS, we can just obtain the different pulsation modes' period changes with same signs and scales.

As we know, the evolutionary effect is originated from the core nuclear reaction, and propagate from inner to outer of the stellar. So we can conclude the evolution of the exterior is later than it of interior. In the theory of stellar pulsation, the domain of fundamental mode pulsation is deeper (more close to the core) than first overtone mode pulsation. Or we can say that the fundamental mode is more sensitive than the first overtone mode to the effect of evolution.

Hence, when the evolution state of the interior of the star pass through the second turn-off on the tracks (Figure 8), the exterior of the star is still in the state between the two turn-offs and preparing to pass through the second turn-off.

With the discussion above, one can explain the different signs of the period changes of the two pulsation modes, and conclude that AE UMa is located just after the second turn-off on the evolutionary tracks (see Figure 8 and Figure 9). Its corresponding mass ranges from $1.68 M_{\odot}$ to $1.80 M_{\odot}$, age from $1.23 \times 10^9 yr$ to $1.51 \times 10^9 yr$.

6. CONCLUSIONS

With the photometric observation data from 2009 to 2012 obtained at Xionglong Station of NAOC, we analyzed the pulsations of AE UMa and resolved up to 37 frequencies, 25 of which are newly detected. All these frequencies are shown to be harmonics or combinations of the two main frequencies $f_0 = 11.62560 c d^{-1}$ and $f_1 = 15.03123 c d^{-1}$, corresponding to the fundamental and the first overtone modes.

A new $O - C$ diagram was constructed with the 84 times of maximum light determined from our new observations and those listed in the literature, leading to the updated value of

period $P_0 = 0.0860170781$ *days*. The new ephemeris with a quadratic solution suggests that the fundamental period change rate of AE UMa $(1/P_0)(dP_0/dt) = 5.4(8) \times 10^{-9} \text{ yr}^{-1}$ and the first overtone period change with a rate of $(1/P_1)(dP_1/dt) = -2.84 \times 10^{-8} \text{ yr}^{-1}$. The first value is different from the result obtained by Zhou (2001), but the second is consistent with the value obtained by Pócs & Szeidl (2001) and Zhou (2001).

We calculated models of stars with masses between $1.68 M_\odot$ and $1.88 M_\odot$. With the constraints of the values of f_0 , f_1 , $(1/P_0)(dP_0/dt)$ and $(1/P_1)(dP_1/dt)$, we concluded that AE UMa locate near the second turn-off of the post-MS evolution tracks with the mass $1.72(\pm 0.06) M_\odot$ and the age $1.4(\pm 0.2) \times 10^9 \text{ yr}$. The results of our calculation support the hypothesis that the period variations derived from the observations are mainly a result of the stellar evolution.

More precise spectroscopic observations are needed, with which one can get more accurate values of T_{eff} and $\log g$, and stronger constraints on the stellar models. As a result, one can study details of the evolutionary effect propagating from the inner to the outer layer of the star.

7. Acknowledgments

JSN and JNF acknowledge the support from the National Natural Science Foundation of China (NSFC), through the Grants 10878007 and U1231202. The research is partially supported by the National Basic Research Program of China (973 Program 2013CB834900) and the Fundamental Research Funds for the Central Universities.

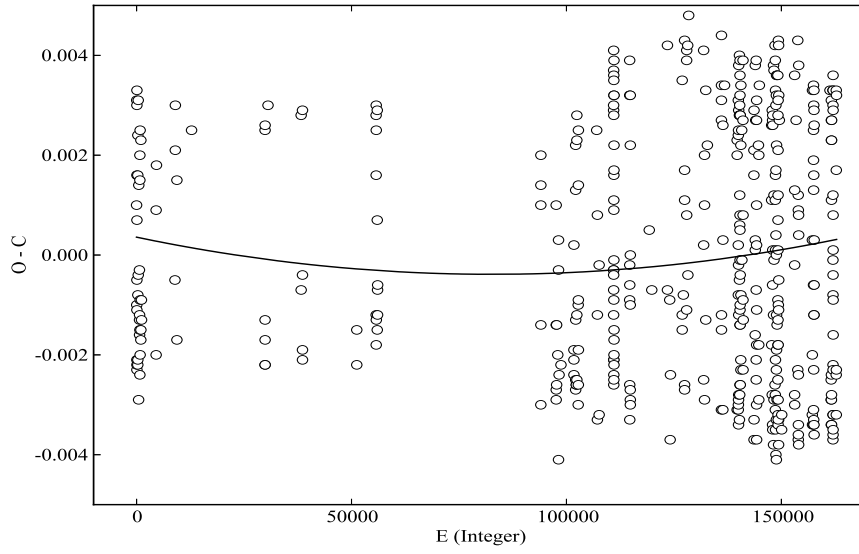


Fig. 5.— $O - C$ diagram of AE UMa. The $O - C$ values are in *days*. E is the cycle number. The solid curve shows the fit concerning a continuous increasing period change

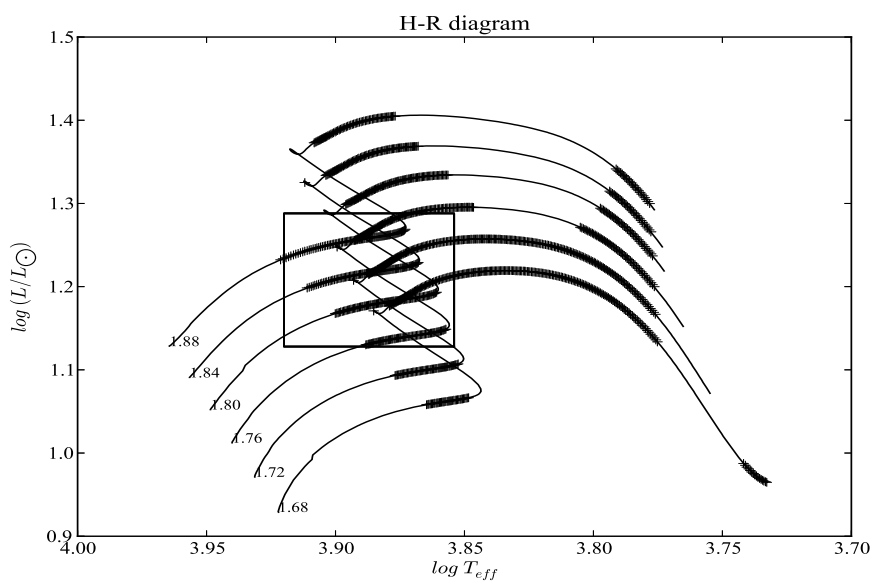


Fig. 6.— Evolutionary tracks of models with mass from $1.68 M_{\odot}$ to $1.88 M_{\odot}$ for $(Y, Z) = (0.25, 0.008521)$. The rectangle shown on the H-R diagram is determined from the observed parameters of AE UMa. Marks on the tracks indicate the evolutionary period changes of $(1/P_0)(dP_0/dt)$ with the value inside the interval $[10^{-9}, 10^{-8}]$ in units of yr^{-1} .

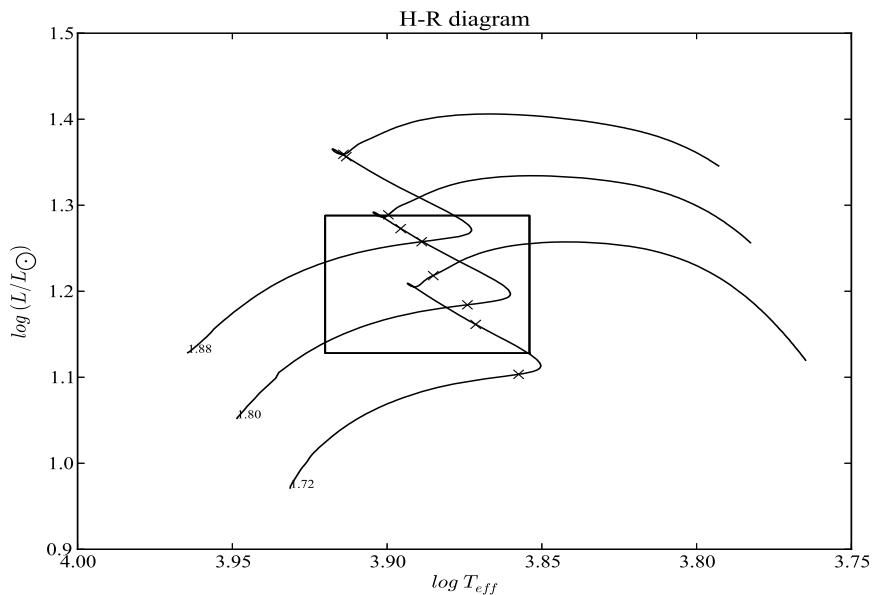
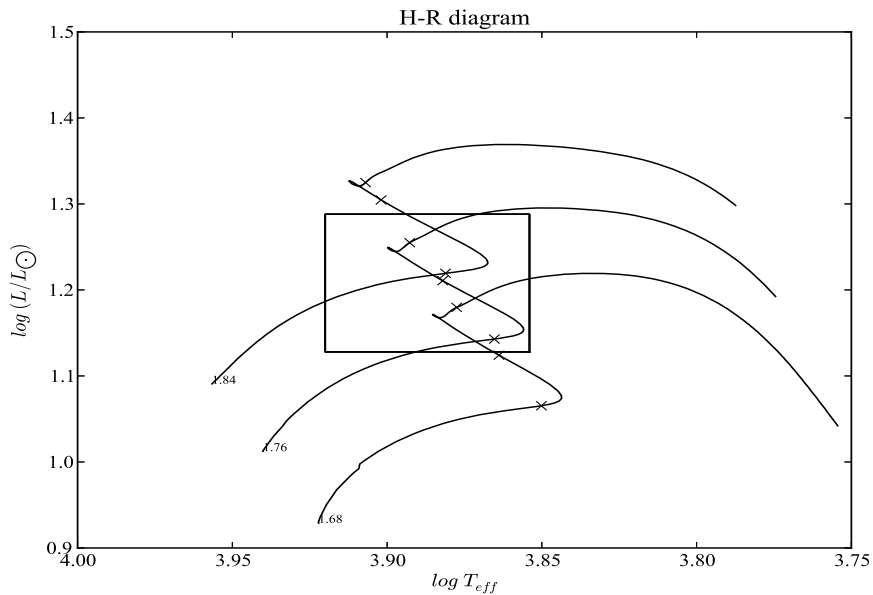
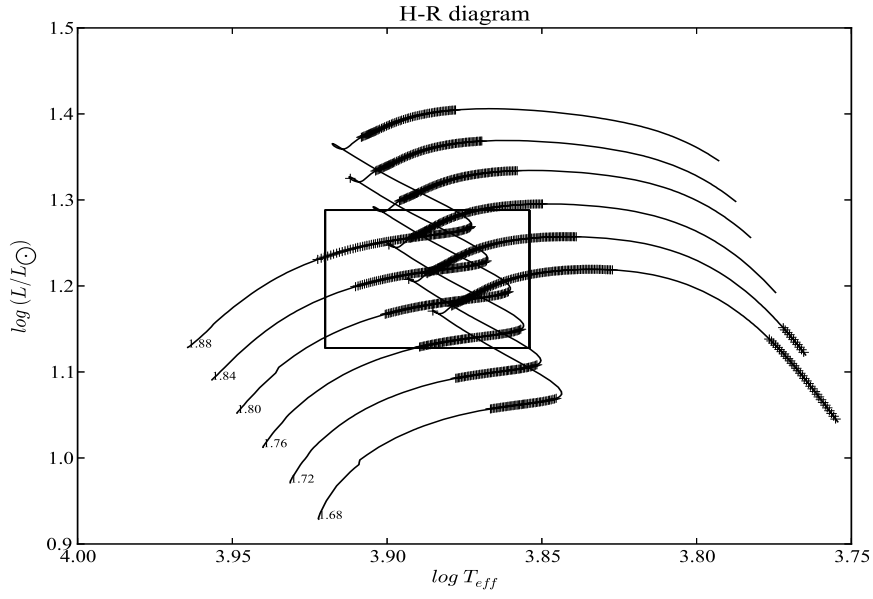
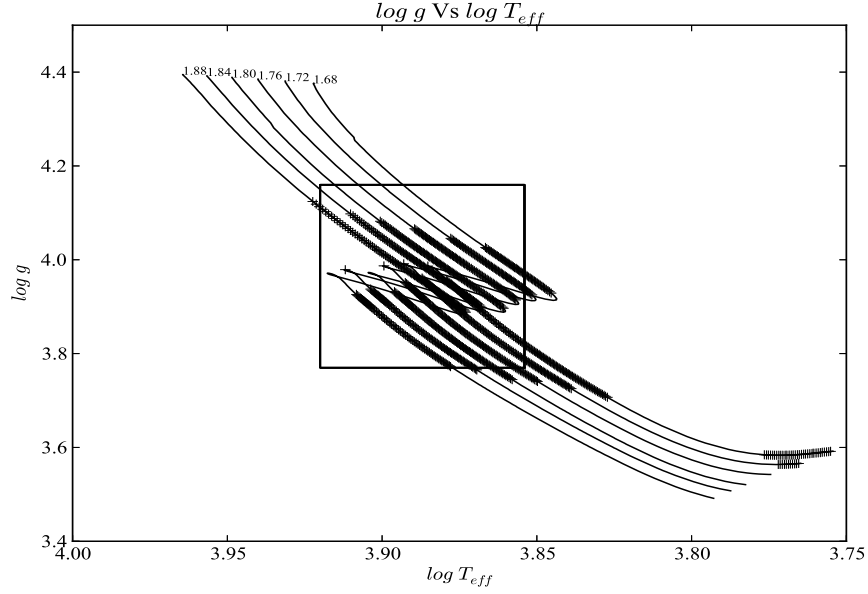


Fig. 7.— Models with f_0 and f_1 calculated with ADIPLS and equal to the observed values are marked on the evolutionary tracks. (a) for mass of $1.68 M_\odot$, $1.76 M_\odot$ and $1.84 M_\odot$; (b) for mass of $1.72 M_\odot$, $1.80 M_\odot$ and $1.88 M_\odot$. In order to see the marks clearly, we divide the results into two figures.

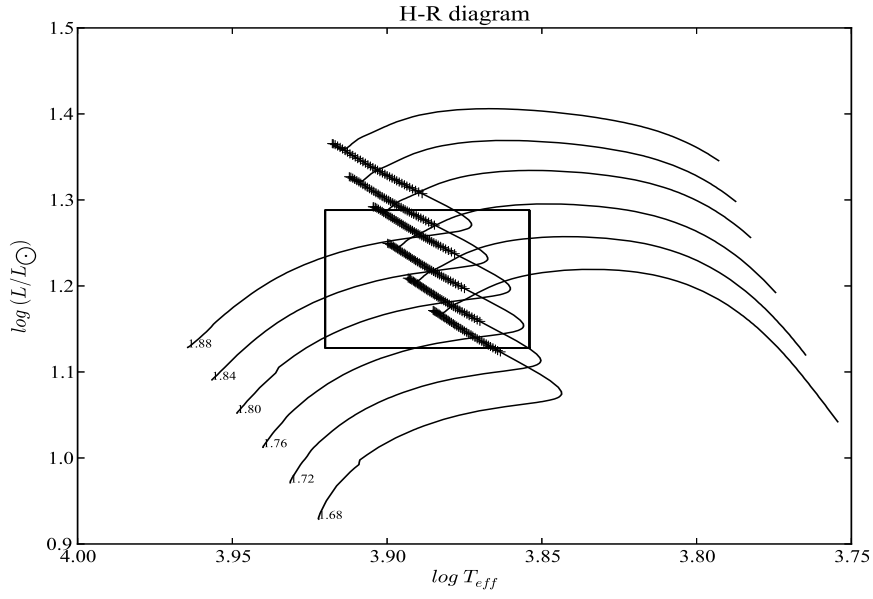


(a)

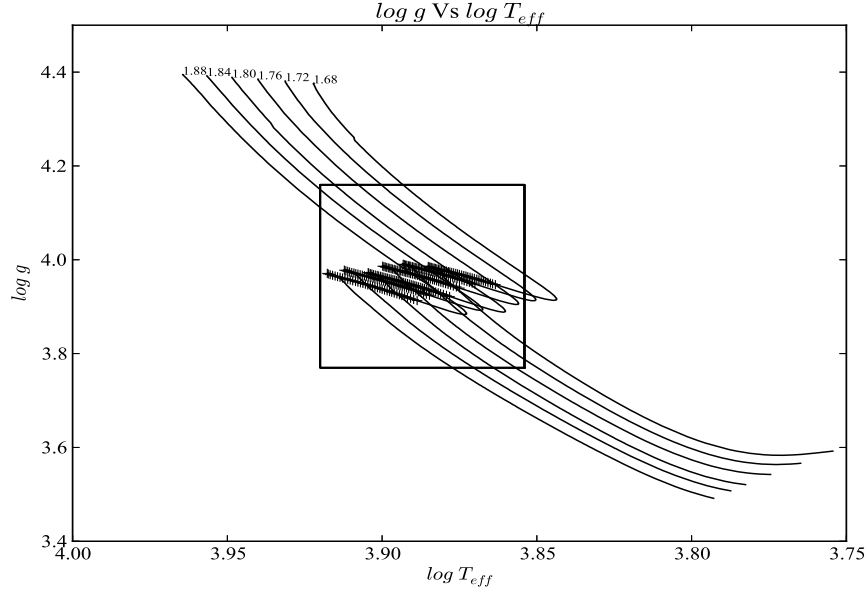


(b)

Fig. 8.— The models for which the variation of the fundamental frequency f_0 calculated with ADIPLS agree with the observed values are marked on the evolutionary tracks. The evolutionary period changes of $(1/P_0)(dP_0/dt)$ are within the interval $[10^{-9}, 10^{-8}]$ in units of yr^{-1} .



(a)



(b)

Fig. 9.— The variation of the first overtone frequency f_1 calculated by ADIPLS are marked in the evolutionary tracks. Marks on the tracks mean the evolutionary period changes as $(1/P_1)(dP_1/dt)$ with the interval $[-10^{-7}, -10^{-8}]$ in units of yr^{-1} .

REFERENCES

- Agerer, F., Dahm, M., & Hubscher, J. 1999a, *Information Bulletin on Variable Stars*, 4712, 1
- Agerer, F., Dahm, M., & Hubscher, J. 1999b, *Information Bulletin on Variable Stars*, 4712, 1
- Agerer, F. & Hubscher, J. 2003, *Information Bulletin on Variable Stars*, 5485, 1
- Braune, W., Huebscher, J., & Mundry, E. 1979, *Astronomische Nachrichten*, 300, 165
- Braune, W. & Mundry, E. 1982, *Berliner Arbeitsgemeinschaft fuer Veraenderliche Sterne - Mitteilungen*, 34
- Breger, M. & Pamyatnykh, A. A. 1998, *A&A*, 332, 958
- Breger, M., Stich, J., Garrido, R., et al. 1993, *A&A*, 271, 482
- Broglia, P. & Conconi, P. 1975, *A&AS*, 22, 243
- Cassisi, S., Potekhin, A. Y., Pietrinferni, A., Catelan, M., & Salaris, M. 2007, *ApJ*, 661, 1094
- Christensen-Dalsgaard, J. 2008, *Ap&SS*, 316, 113
- Claret, A., Rodriguez, E., Rolland, A., & Lopez de Coca, P. 1990, in *Astronomical Society of the Pacific Conference Series, Vol. 11, Confrontation Between Stellar Pulsation and Evolution*, ed. C. Cacciari & G. Clementini, 481
- Crawford, D. L. & Mander, J. 1966, *AJ*, 71, 114
- Ferguson, J. W., Alexander, D. R., Allard, F., et al. 2005, *ApJ*, 623, 585
- Filatov, G. S. 1960, *Astronomicheskij Tsirkulyar*, 215, 20

- Freedman, R. S., Marley, M. S., & Lodders, K. 2008, *ApJS*, 174, 504
- Frommhold, L., Abel, M., Wang, F., et al. 2010, *Molecular Physics*, 108, 2265
- Fu, J.-N., Zhang, C., Marak, K., et al. 2008, *Chinese J. Astron. Astrophys.*, 8, 237
- Garcia, J. R., Cebral, J. R., Scoccimarro, E. R., et al. 1995, *A&AS*, 109, 201
- Geyer, E., Kippenhahn, R., & Strohmeier, W. 1955, Nr, 11
- Girardi, L., Bressan, A., Bertelli, G., & Chiosi, C. 2000, *A&AS*, 141, 371
- Götz, W. & Wenzel, W. 1961, *Sonneberg*, 571
- Hintz, E., Hintz, M. L., & Joner, M. D. 1997a, *PASP*, 109, 1073
- Hintz, E. G., Joner, M. D., McNamara, D. H., et al. 1997b, *PASP*, 109, 15
- Hubscher, J. 2005, *Information Bulletin on Variable Stars*, 5643, 1
- Hubscher, J. 2007, *Information Bulletin on Variable Stars*, 5802, 1
- Hübscher, J., Agerer, F., & Wunder, E. 1992, *Berliner Arbeitsgemeinschaft fuer
Veraenderliche Sterne - Mitteilungen*, 60, 1
- Hubscher, J., Lehmann, P. B., Monninger, G., Steinbach, H.-M., & Walter, F. 2010,
Information Bulletin on Variable Stars, 5918, 1
- Hubscher, J., Paschke, A., & Walter, F. 2005, *Information Bulletin on Variable Stars*, 5657,
1
- Hubscher, J., Paschke, A., & Walter, F. 2006, *Information Bulletin on Variable Stars*, 5731,
1

- Hubscher, J., Steinbach, H.-M., & Walter, F. 2009, *Information Bulletin on Variable Stars*, 5874, 1
- Hubscher, J. & Walter, F. 2007, *Information Bulletin on Variable Stars*, 5761, 1
- Huebscher, J., Lichtenknecker, D., & Mundry, E. 1985, *Berliner Arbeitsgemeinschaft fuer Veraenderliche Sterne - Mitteilungen*, 39
- Huebscher, J. & Monninger, G. 2011, *Berliner Arbeitsgemeinschaft fuer Veraenderliche Sterne - Mitteilungen*, 214, 1
- Klingenberg, G., Dvorak, S. W., & Robertson, C. W. 2006, *Information Bulletin on Variable Stars*, 5701, 1
- Lenz, P. & Breger, M. 2005, *Communications in Asteroseismology*, 146, 53
- Paxton, B., Bildsten, L., Dotter, A., et al. 2011, *ApJS*, 192, 3
- Paxton, B., Cantiello, M., Arras, P., et al. 2013, *ArXiv e-prints*
- Pejcha, O., Havlik, T., & Kral, L. 2001, *Information Bulletin on Variable Stars*, 5080, 1
- Pócs, M. D. & Szeidl, B. 2001, *A&A*, 368, 880
- Poretti, E. 2003, *A&A*, 409, 1031
- Potekhin, A. Y. & Chabrier, G. 2010, *Contributions to Plasma Physics*, 50, 82
- Rodríguez, E. & Breger, M. 2001, *A&A*, 366, 178
- Rodríguez, E., López de Coca, P., Costa, V., & Martín, S. 1995, *A&A*, 299, 108
- Rodríguez, E. & López-González, M. J. 2000, *A&A*, 359, 597

Rodriguez, E., Rolland, A., Lopez de Coca, P., Garcia-Lobo, E., & Sedano, J. L. 1992, A&AS, 93, 189

Samolyk, G. 2010, Journal of the American Association of Variable Star Observers (JAAVSO), 38, 12

Strömgren, B. 1956, Vistas in Astronomy, 2, 1336

Szeidl, B. 1974, Information Bulletin on Variable Stars, 903, 1

Tsesevich, V. P. 1973, Astronomicheskij Tsirkulyar, 775, 2

Yang, X. H., Fu, J. N., & Zha, Q. 2012, AJ, 144, 92

Yurchenko, S. N., Barber, R. J., & Tennyson, J. 2011, MNRAS, 413, 1828

Zhou, A.-Y. 2001, A&A, 374, 235

Zhou, A.-Y., Jiang, X.-J., Zhang, Y.-P., & Wei, J.-Y. 2009, Research in Astronomy and Astrophysics, 9, 349